CONDENSED MATTER PHYSICS

Electrically driven photon emission from individual atomic defects in monolayer WS_2

Bruno Schuler[1]*†, Katherine A. Cochrane[1], Christoph Kastl[1,2], Edward S. Barnard[1], Edward Wong[1], Nicholas J. Borys[1,3], Adam M. Schwartzberg[1], D. Frank Ogletree[1], F. Javier García de Abajo[4,5]†, Alexander Weber-Bargioni[1]†

Copyright © 2020 The Authors, some rights reserved; exclusive licensee American Association for the Advancement of Science. No claim to original U.S. Government Works. Distributed under a Creative Commons Attribution NonCommercial License 4.0 (CC BY-NC).

Quantum dot–like single-photon sources in transition metal dichalcogenides (TMDs) exhibit appealing quantum optical properties but lack a well-defined atomic structure and are subject to large spectral variability. Here, we demonstrate electrically stimulated photon emission from individual atomic defects in monolayer WS_2 and directly correlate the emission with the local atomic and electronic structure. Radiative transitions are locally excited by sequential inelastic electron tunneling from a metallic tip into selected discrete defect states in the WS_2 bandgap. Coupling to the optical far field is mediated by tip plasmons, which transduce the excess energy into a single photon. The applied tip-sample voltage determines the transition energy. Atomically resolved emission maps of individual point defects closely resemble electronic defect orbitals, the final states of the optical transitions. Inelastic charge carrier injection into localized defect states of two-dimensional materials provides a powerful platform for electrically driven, broadly tunable, atomic-scale single-photon sources.

INTRODUCTION

Solid-state quantum emitters are promising building blocks for quantum technologies such as high-precision sensing and secure communications (*1*). In particular, atom-like emitters embedded in a host crystal [e.g., color centers in diamond (*2*) and silicon carbide (SiC) (*3*)] combine several appealing properties, namely, spin-selective optical transitions (*2*), room temperature stability (*4*), exceptionally long coherence times (*4*), and potential for scalability (*5*). However, on demand integration of quantum emitters with well-defined optical characteristics remains an unsolved challenge in solid-state quantum photonics. The development of these key capabilities requires achieving high-precision spatial placement; controlling the mesoscopic environment to avert variability between emitters; identifying and eliminating decoherence channels; and developing high-fidelity, scalable pumping schemes that are amenable to on-chip integration, such as electrically driven optical emission (*1*).

Two-dimensional (2D) materials are emerging as a powerful platform for hosting next-generation quantum emitters (*1*, *6*), excelling in synthetic flexibility (*7*), high photon extraction efficiency (*1*), and tunability through external gates and substrate engineering (*8*). They also provide unparalleled control of emitter placement (*9*) and integration with photonic (*10*) and plasmonic (*11*) nanocavities. Various quantum emitters have been recently discovered in semiconducting transition metal dichalcogenides (TMDs) such as tungsten diselenide (WSe_2) (*12*–*17*) and molybdenum diselenide ($MoSe_2$) (*18*). While the exact origin of the emission is still actively debated, the single-photon emission has been attributed to a quantum dot–like confinement of excitons down to tens of nanometers (*14*), for instance, due to residual strain from the material transfer process (*12*). These quantum dot–like mesoscopic 2D emitters are structurally not well defined and exhibit large spectral variability, thus precluding their identical generation and precise spatial placement. These are the main challenges that prevent a systematic development and deployment of quantum emitters in 2D materials.

Here, we demonstrate photon emission from individual atomic defects in epitaxially grown monolayer tungsten disulfide (WS_2) driven by local electron injection from a Au-coated tip. We correlate the atomic structure, electronic structure, and photon emission of the exact same defects with atomic spatial resolution. Specifically, we demonstrate on demand photon emission from intrinsic tungsten substitutes and deliberately created sulfur vacancies (Vac_S) by local electrical stimulation. We use a plasmonic scanning tunneling tip to drive optical transitions by sequential inelastic tunneling, tune the emission via the applied bias voltage, and map the photon emission from individual defect orbitals with the highest spatial resolution so far reported on par with that obtained using conventional elastic scanning tunneling microscopy (STM).

RESULTS AND DISCUSSION

Single-defect luminescence in monolayer WS_2 is driven by electron tunneling from a plasmonic scanning probe tip (Fig. 1A). Through precise tip positioning, assisted by an extremely local electron transfer mechanism, we can selectively excite a single defect, free from any background luminescence of the host crystal. Electrons injected from the continuum of metallic tip states into discrete defect states of the 2D material generate broad optical emission spectra, with associated photon energies corresponding to the difference between initial (tip) and final (defect) electron energies in the tunneling process (Fig. 1B). The metal tip acts as a plasmonic antenna that assists the coupling between the inelastic tunneling current and the far-field light emission. This allows us to control the emitted photon energy through the applied tip-sample bias voltage, resulting in emission rates directly proportional to the electron density in the defect orbital right under the tip position.

[1]Molecular Foundry, Lawrence Berkeley National Laboratory, CA 94720, USA. [2]Walter-Schottky-Institut and Physik-Department, Technical University of Munich, Garching 85748, Germany. [3]Department of Physics, Montana State University, Bozeman, MT 59717, USA. [4]ICFO-Institut de Ciències Fotòniques, The Barcelona Institute of Science and Technology, 08860 Castelldefels, Barcelona, Spain. [5]ICREA-Institució Catalana de Recerca i Estudis Avançats, 08010 Barcelona, Spain.
*Present address: nanotech@surfaces Laboratory, Empa, Swiss Federal Laboratories for Materials Science and Technology, Dübendorf, Switzerland.
†Corresponding author. Email: bruno.schuler@empa.ch (B.S.); javier.garciadeabajo@nanophotonics.es (F.J.G.A.); afweber-bargioni@lbl.gov (A.W.-B.)

Downloaded from http://advances.sciencemag.org/ on October 19, 2020

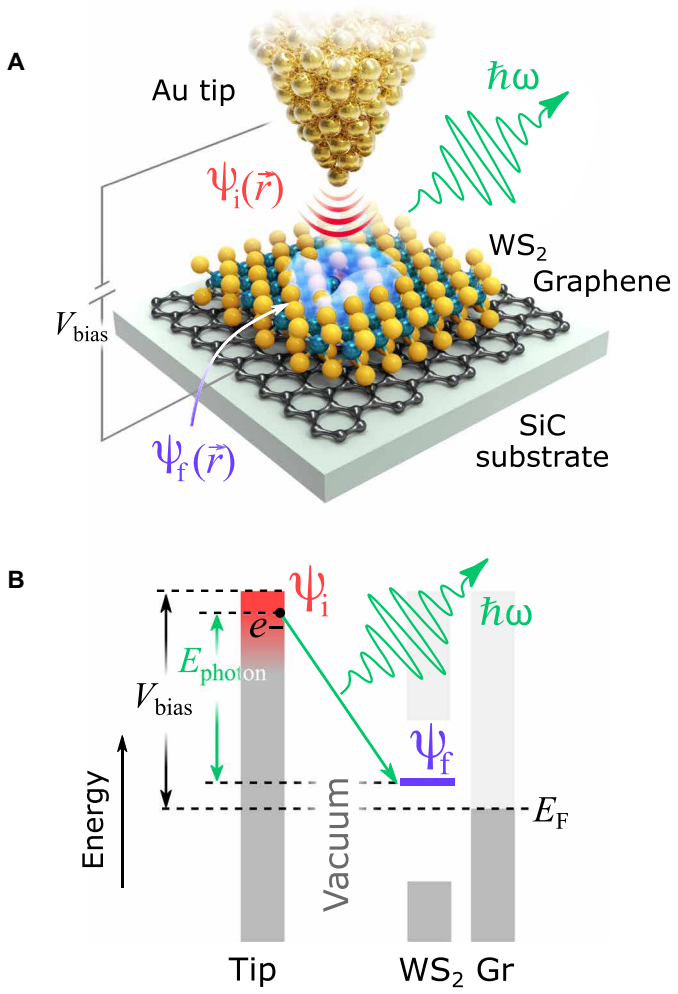

Fig. 1. Tunneling electron-induced photon emission. Scheme of experimental configuration (**A**) and electron energy levels (**B**) involved in electrically driven photon emission from an atomic point defect. An electron from a gold tip (initial state ψ_i in red) tunnels inelastically into an atomic defect (top sulfur vacancy) of monolayer WS_S (final state ψ_f in purple). The excess of transition energy $\hbar\omega$ is released into the emission of one photon, mediated by intermediate plasmon states of the tip cavity. The 2D material is supported on a graphene layer (electric contact) on top of SiC. The tip-sample bias voltage V_{bias} controls the electron injection energy. An inelastic electron transition is represented by the green downward pointing arrow in (B). The dark and light gray boxes represent filled and empty states, respectively. Photo credit: Ignacio Gaubert

Our single-atom system is fundamentally different from previous reports of mesoscale emitters in 2D materials. All atomic emitters in our study are identical because they have an atomically well-defined structure and very localized electronic wave functions that are much less susceptible to long-range disorder, such as strain or neighboring structural defects. Our observations are fully reproducible when looking at different defects of the same nature. In our experiments, we only observe local relaxation of the lattice in the immediate vicinity of the defect (*19*). Mesoscopic strain potentials can be excluded because the samples are grown by van der Waals epitaxy and not obtained by exfoliation (*19*, *20*). In addition, atomic defects in TMDs can be generated with high-density control and specificity, for instance, through chemical doping or by annealing, as we show in this work.

We use the Au-coated tip of a STM to inject charge carriers and mediate the coupling between optical near and far fields via tip plasmon modes. This so-called STM luminescence (STML) emission (*21*) has been successfully exploited in studies of metallic surfaces (*22*) and molecular systems (*23*) to beat the light diffraction limit by more than two orders of magnitude due to the extreme localization of initial and final electron states in the tunneling process. In this context, electroluminescence from single molecules has been recently established through self-decoupling (*24*) or by introducing ultrathin insulating layers (*25*) between the molecule and a noble metal substrate. In addition, STML has enabled vibronic spectroscopy with submolecular resolution (*25*, *26*), imaging molecular orbitals through photon emission maps (*27*, *28*), studying charge and exciton dynamics (*24*, *29*, *30*), and stimulating spin-selective optical transitions (*31*). STML on indium tin oxide–supported $MoSe_2$ has also been recently reported and attributed to radiative decay of the A exciton in this material (*32*).

Plasmonic noble metal substrates, which are commonly used in STML, are not a viable option to investigate TMDs because strong hybridization quenches the intrinsic optical emission (*33*). Instead, we use epitaxial graphene grown on SiC as a substrate, which has been shown to preserve the native TMD band structure (*20*). While electroluminescence from graphene has been previously observed (*34*), we find conclusive evidence to assign the optical emission in our TMD/graphene heterostructure to the electronic states of the TMD alone.

We prepare our samples by growing monolayer WS_2 islands on epitaxial graphene on SiC using chemical vapor deposition (*20*). The as-grown sample contains several substitutional atomic defects, such as chromium (Cr_W) and molybdenum (Mo_W) replacing tungsten, as well as oxygen substituting sulfur (O_S) (*19*, *35*). Then, we selectively generate Vac_S in both the top and bottom sulfur layers by high-temperature annealing in vacuum (*36*). Both Cr_W and Vac_S defects exhibit unoccupied electronic states placed a few hundred millielectronvolts below the WS_2 conduction band edge (Fig. 2B) (*19*, *36*). Elastic tunneling into these in-gap defect states gives rise to pronounced resonances in the differential conductance (dI/dV) spectra measured in scanning tunneling spectroscopy (STS), which roughly yields the local density of states, as shown in Fig. 2E. Their characteristic electronic spectrum results from a combination of crystal field splitting, spin-orbit coupling, and electron-phonon interaction (*19*).

At tunneling voltages exceeding 1.5 V, we observe electron-induced photon emission originating from inelastic electron tunneling on the Cr_W and Vac_S defects, as well as on defect-free WS_2 locations. The emission rate strongly depends on the applied bias and position (e.g., on or off a defect, as well as different regions within the defect) where STML spectra are acquired at constant current, as shown in Fig. 2F. We find a clear correlation between the bias onset for photon emission and the energy of the lowest unoccupied states observed in dI/dV. In particular, the difference between the bias onset of Vac_S (2.2 V) and Cr_W (2.4 V) is 0.2 V, which agrees with the energy difference of their respective defect states. Similarly, we observe STML at negative bias polarities (hole injection), for which the emission onset relates to the energy of the highest occupied state (see fig. S7). The emission scales linearly with the current, thus suggesting a single-electron process. In what follows, we focus on photon emission from sulfur top vacancies. Similar results for Cr_W can be found in the Supplementary Materials.

The extremely localized excitation by tunneling electron injection allows us to record atomically resolved photon maps. In Fig. 3A, we

Downloaded from http://advances.sciencemag.org/ on October 19, 2020

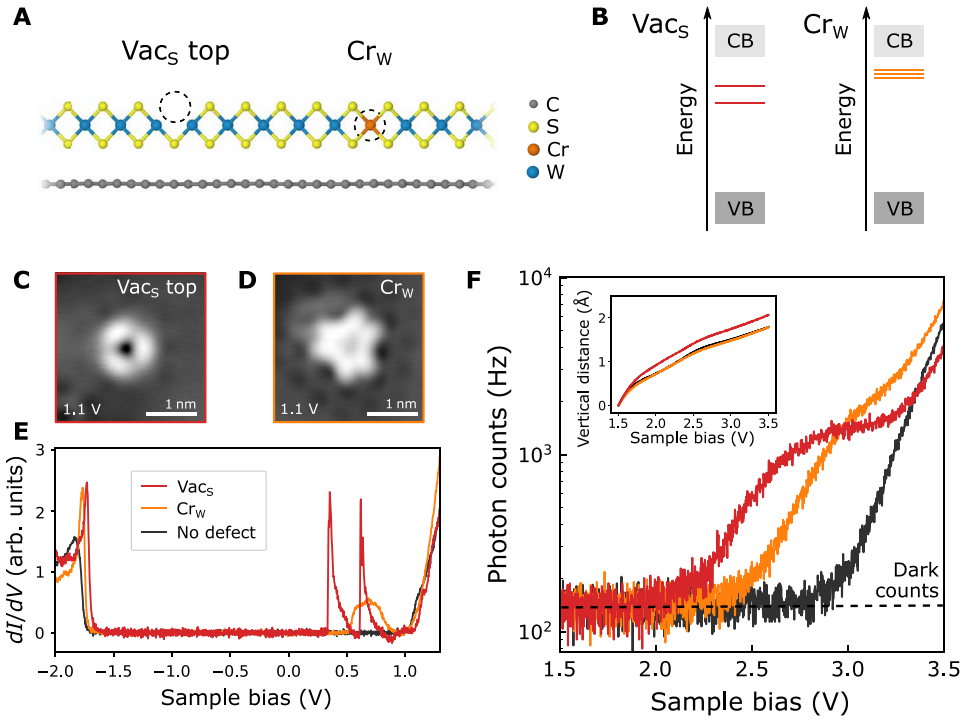

Fig. 2. Tunneling bias dependence of photon emission. (**A**) Side view of atomic layers and the two types of WS_2 defects that we study here: a top sulfur vacancy (Vac_S top) and a chromium substituting tungsten (Cr_W). (**B**) Energy level diagrams showing the two unoccupied Vac_S defect states (red) and three unoccupied Cr_W defect states (orange), lying in the gap between valence and conduction bands (VB and CB). (**C** and **D**) STM topography (constant current $I = 20$ pA and bias $V = 1.1$ V) of Vac_S top (C) and Cr_W (D). (**E**) We probe the local density of states through dI/dV spectroscopy on Vac_S (red) and Cr_W (orange) defects compared with a position far from any defect (gray). The dI/dV spectra of top and bottom Vac_S are identical (*36*). (**F**) Spectrally integrated photon emission induced by inelastic electron tunneling at constant current $I = 10$ nA. Measurements in (E) and (F) were recorded at the same defect sites and with the same tip.

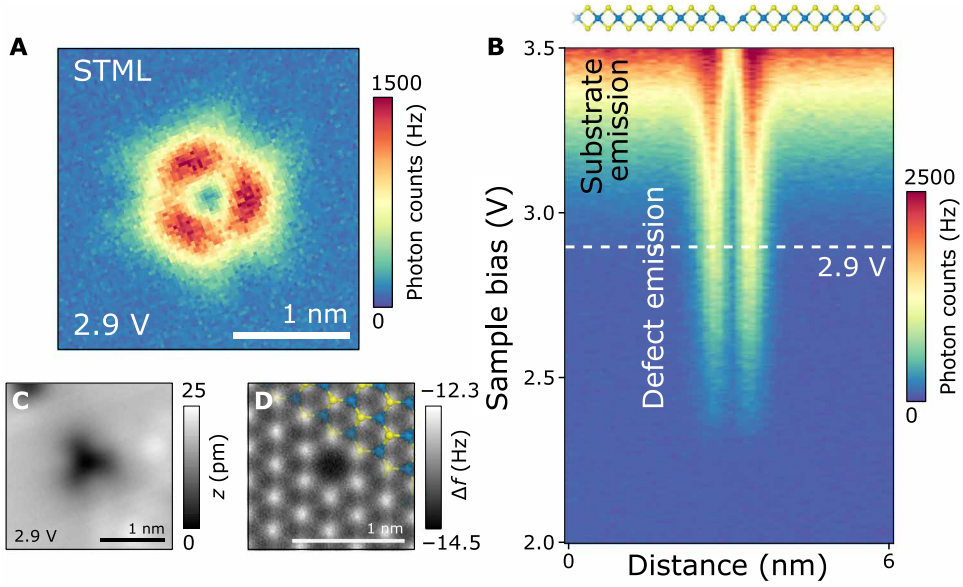

Fig. 3. Photon emission spatial imaging of a single sulfur vacancy. (**A**) Spectrally integrated photon map of a Vac_S top defect acquired with $I = 20$ nA constant current and $V = 2.9$ V bias. This map is in excellent agreement with the STM image of the in-gap defect orbital (see Fig. 2C). (**B**) Spectrally integrated photon emission across Vac_S top as a function of tunneling bias. The white dashed line indicates the bias at which the map in (A) was acquired. The defect exhibits strongly localized photon emission at a tunneling bias substantially lower than the onset of substrate emission. (**C**) STM topography of Vac_S top simultaneously acquired during the photon map shown in (A). (**D**) CO tip noncontact atomic force microscopy (nc-AFM) image of a Vac_S top.

Downloaded from http://advances.sciencemag.org/ on October 19, 2020

show the spectrally integrated photon emission as a function of lateral tip position over a single Vac_S in the top sulfur layer. The subnanometer-resolved photon maps acquired at high biases closely resemble the STM image of the in-gap defect orbital (Fig. 2C). The emission does not correlate with the simultaneously acquired STM topography at high bias (Fig. 3C), therefore excluding any substantial effect of the slightly varying gap distance on the spatial variation of the emission. Laterally, the defect emission is closely confined within ~1 nm, concurrent with the electronic orbital dimensions (see Fig. 3B).

The close resemblance between the STM map resonant with the defect state and the STML map is further supported by theory. Photon emission in STML is mediated by the transition dipole $\boldsymbol{p}$ associated with the tunneling electron, acting as a radiation source (*37*) and giving rise to an emission yield $\propto |\boldsymbol{p}|^2$, which is, in turn, proportional to the elastic tunneling current measured in STM (see details in the Supplementary Materials). This current alone bears a dependence on the sampled final state, and therefore, both elastic and inelastic tunneling rates are proportional to the electron density of states at the tip position, given by the defect orbital density $|\psi_f|^2$. Similar to the enhanced emission rate of an excited atom in a resonant cavity defined by the Purcell factor $P(\omega)$, the spectrally resolved STML rate is directly proportional to $P(\omega)$, which, for metallic tips, is dominated by light-plasmon coupling and can be observed through optical spectroscopy.

Spectrally resolved STML measurements on the sulfur vacancy defect shown in Fig. 4 reveal broadband photon emission. The large spectral width originates from the finite energy range of tunneling electrons from the metallic tip (cf. Fig. 1B) and is not related to the intrinsic broadening of the defect state or the plasmonic near-field amplification by the tip. We find that the detected far-field spectra generally extend to 2.0 to 2.3 eV, which is consistent with the calculated field enhancement $P(\omega)$ between a spherical Au tip and the SiC substrate (fig. S3). At low photon energies, losses in the W tip (~1 eV) and reduced quantum yield of the photon detectors (~1.2 eV) produce a cutoff in the spectrum. The Purcell enhancement, and hence the spectral shape of the luminescence, is determined by the tip morphology and material. While broad luminescence results from the continuum of tip states and not the plasmonic enhancement, the latter weights the inelastic electron transitions by the photon density of states, which can introduce changes in the detailed spectral profile and actual intensity of the emission. We refer the reader to the Supplementary Materials for a detailed theoretical analysis of the near-field enhancement as a function of tip material and morphology, as well as luminescence spectra recorded with different tips including a comparison of W and Ag bulk tip wires.

We can identify two distinct regions in the plot of the emission intensity as a function of photon energy and tunneling bias (Fig. 4B): the high-bias, low photon energy corner (top left) is associated with substrate emission from WS_2 (i.e., tunneling to substrate states), while the distinct emission band at lower bias is associated exclusively with the defect. For Vac_S, two emission steps (marked by white arrows in Fig. 4B) are observed, which follow a linear relation between applied bias and photon energy. Each of these steps corresponds to the opening of a new radiative decay channel, which we attribute to a transition from tip states at or below its Fermi level into the two unoccupied sulfur vacancy states. At the threshold energies indicated by the white arrows in Fig. 4B, the entire potential energy of the tunneling electron across the vacuum barrier is converted into a photon with matching energy, hence suggesting a single-electron to single-photon conversion mechanism. Figure 4C shows these transitions for a specific photon energy $\hbar\omega = 1.85$ eV, with each new decay channel indicated in the insets. Emission of a single photon associated with a single-electron transition is the dominant lowest-order radiative process. Accordingly, the highest allowed photon energy is given by the difference between the tip Fermi energy and the defect state energy.

For our Au-coated tungsten tips, we detect $\sim 10^{-7}$ far-field photons per electron. Accounting for all setup related losses, the intrinsic quantum efficiency of the radiative tunneling process is estimated as $Y \sim 10^{-4}$ photons per electron. It is interesting to compare this

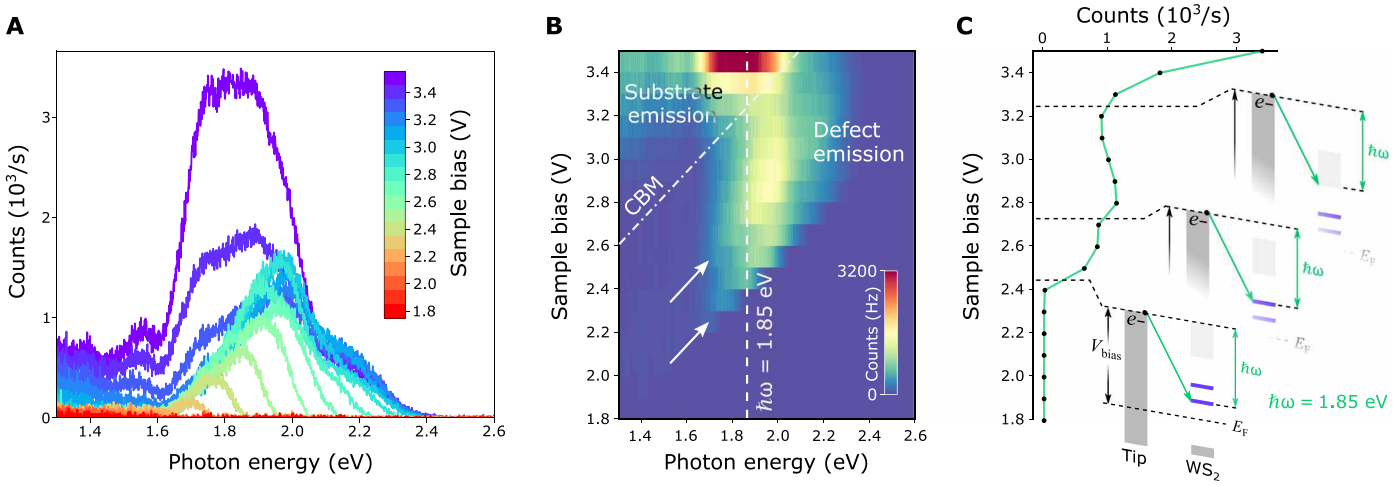

Fig. 4. Spectrally resolved photon emission on a single sulfur vacancy. (**A**) Photon emission spectrum on Vac_S at different tunneling biases. The spectral width and the minimal spectral variation with lateral tip position suggest a plasmon-mediated emission process. (**B**) 2D representation of the data in (A). Oblique arrows indicate transitions into the two discrete Vac_S defect states. The oblique dashed line marks the onset of substrate emission corresponding to inelastic tunneling into the WS_S conduction band minimum (CBM). (**C**) Photon counts at $\hbar\omega = 1.85$ eV [cut along the vertical dashed line in (B)]. We identify two emission onsets corresponding to inelastic transitions into the lower and higher Vac_S defect state, as well as a higher-energy onset assigned to transitions into the WS_S CBM.

Downloaded from http://advances.sciencemag.org/ on October 19, 2020

number with the analytical result (see Supplementary Materials) $Y \sim (3\pi\alpha/2)(d/\lambda)^2(\Delta\omega/\omega)P(\omega)$, where ω, λ, and Δω are the photon frequency, wavelength, and bandwidth, respectively; d is the tip-sample distance; and $\alpha \approx 1/137$ is the fine-structure constant. The Purcell factor P, which scales linearly with the density of available optical states dominated by plasmon modes in the tip-sample nanocavity (*38*), can be estimated by invoking electromagnetic reciprocity, asserting that the emission intensity is strictly proportional to the enhancement in the near-field intensity under external illumination at the position of the emitting dipole. The latter depends on the precise tip-sample morphology but is rather insensitive to the lateral position of the tip in the nonmetallic SiC substrate under consideration and reaches plasmon-enhanced values of $P \sim 10^4$ (see the Supplementary Materials). Using parameters corresponding to our experimental conditions, we then predict a photon yield per tunneled electron $Y \sim 10^{-4}$ in good agreement with the experimental estimate.

Ultimately, the photon generation rate is fundamentally limited by Coulomb blockade, which prevents tunneling of subsequent electrons into the defect state before the previous electron drains to the graphene substrate. Accordingly, the correlation time of single-photon emission events as derived by the antibunching in a $g^{(2)}(t)$ experiment is expected to yield this Coulomb blockade time, as also suggested by recent STML experiments for C_{60} multilayers on Ag (*39*). From the dI/dV linewidth of the vacancy state of 8 meV, we estimate a lower bound of the transient charging time of the defect on the order of 100 fs. This number is well beyond the time resolution of state-of-the-art timing electronics in a $g^{(2)}(t)$ measurement. Hence, the single-photon character in our experiments can only be inferred indirectly through the sequential single-electron tunneling and the matching electron-to-photon conversion energy. We note that the Coulomb blockade time could be exponentially increased by introducing a tunneling barrier between the TMD layer and the graphene substrate, to attain a measurable $g^{(2)}(t)$ lifetime in the future. Conversely, a short Coulomb blockade time enables a high single-photon generation rate. In our case, a 100-fs lifetime and 10^{-4} conversion yield suggest that a 10^9 Hz single-photon generation rate should be attainable. This number can be even increased using optimized plasmonic or optical cavities to enhance the Purcell factor.

CONCLUSION

In conclusion, we demonstrate electrically induced photon emission from individual, atomically defined defects in a 2D semiconductor. Atomically resolved luminescence maps from deliberately introduced sulfur vacancy defects and native Cr_W substituents reveal that the in-gap defect orbitals are the final states of the optical transition. Electrons that tunnel inelastically from a continuum of tip states into discrete defect states can convey their excess transition energy into plasmonic excitations in the tip nanocavity, mediating their coupling to propagating photons. The widely tunable optical emission generated by charge carrier injection into localized defect states in a 2D material is a powerful platform for electrically driven single-photon emission. The single-defect/single-electron/single-photon regime allows us to avoid averaging and environmental decoherence effects. Monochromatic electron injection, for instance, using a superconducting electrode and charge state control of the defect by gating, could eventually enable on demand spin-polarized single-photon emission in a solid-state tunneling device.

MATERIALS AND METHODS

STM/STS and CO tip nc-AFM measurements

All scanning probe measurements were conducted at low-temperature ($T \approx 6$ K) and ultrahigh vacuum pressure ($P \approx 10^{-10}$ mbar). STM images were recorded using constant-current feedback. STS spectra were performed in constant height mode with a 5-mV lock-in amplitude. The bias voltage was applied to the sample.

For the noncontact atomic force microscopy (nc-AFM) measurements, a qPlus (*40*) quartz-crystal cantilever was used (resonance frequency, $f_0 \approx 30$ kHz; spring constant, $k \approx 1800$ N/m; quality factor, $Q \approx 30{,}000$; and oscillation amplitude, $A \approx 1$ Å). The metallic tip was functionalized with a CO molecule for enhanced resolution (*41*).

STM luminescence

For the STML measurements, we used constant-current STM feedback to drive a constant electron flux at varying tunneling biases at a specific location on the sample. The emitted light was collimated using a high numerical aperture, achromatic lens close to the tunneling junction. Outside the vacuum chamber, the light was refocused into an optical fiber to guide it to a point detector or spectrometer. A photon multiplier tube (Hamamatsu, H7421-50) and a grating spectrometer (Princeton Instruments, SpectraPro 2300i) with a thermoelectrically cooled charge-coupled device photodetector (Andor, Newton) were used. The STML spetra were measured using a 150 grooves per millimeter grating and were not corrected for the wavelength-dependent detection efficiency.

Tip preparation

All measurements shown in the manuscript were taken with an electrochemically etched W wire. We applied in vacuo high-voltage (~80 V) field emission and indentations on a Au(111) single crystal to sharpen the tip. This resulted in a Au-coated apex as shown in the scanning electron microscopy/energy-dispersive x-ray data in fig. S9. More information on the tip dependence of STML can be found in the Supplementary Materials.

SUPPLEMENTARY MATERIALS

Supplementary material for this article is available at http://advances.sciencemag.org/cgi/content/full/6/38/eabb5988/DC1

REFERENCES AND NOTES

1. I. Aharonovich, D. Englund, M. Toth, Solid-state single-photon emitters. *Nat. Photonics* **10**, 631–641 (2016).
2. A. Gruber, A. Dräbenstedt, C. Tietz, L. Fleury, J. Wrachtrup, C. von Borczyskowski, Scanning confocal optical microscopy and magnetic resonance on single defect centers. *Science* **276**, 2012–2014 (1997).
3. S. Castelletto, B. C. Johnson, V. Ivády, N. Stavrias, T. Umeda, A. Gali, T. Ohshima, A silicon carbide room-temperature single-photon source. *Nat. Mater.* **13**, 151–156 (2014).
4. P. C. Maurer, G. Kucsko, C. Latta, L. Jiang, N. Y. Yao, S. D. Bennett, F. Pastawski, D. Hunger, N. Chisholm, M. Markham, D. J. Twitchen, J. I. Cirac, M. D. Lukin, Room-temperature quantum bit memory exceeding one second. *Science* **336**, 1283–1286 (2012).
5. W. F. Koehl, H. Seo, G. Galli, D. D. Awschalom, Designing defect spins for wafer-scale quantum technologies. *MRS Bull.* **40**, 1146–1153 (2015).
6. K. F. Mak, J. Shan, J.han, Photonics and optoelectronics of 2D semiconductor transition metal dichalcogenides. *Nat. Photonics* **10**, 216–226 (2016).
7. S. Das, J. A. Robinson, M. Dubey, H. Terrones, M. Terrones, Beyond graphene: Progress in novel two-dimensional materials and van der Waals solids. *Annu. Rev. Mater. Res.* **45**, 1–27 (2015).
8. K. S. Novoselov, A. Mishchenko, A. Carvalho, A. H. C. Neto, 2D materials and van der Waals heterostructures. *Science* **353**, aac9439 (2016).
9. J. Klein, M. Lorke, M. Florian, F. Sigger, L. Sigl, S. Rey, J. Wierzbowski, J. Cerne, K. Müller, E. Mitterreiter, P. Zimmermann, T. Taniguchi, K. Watanabe, U. Wurstbauer, M. Kaniber,

Downloaded from http://advances.sciencemag.org/ on October 19, 2020

M. Knap, R. Schmidt, J. J. Finley, A. W. Holleitner, Site-selectively generated photon emitters in monolayer MoS_2 via local helium ion irradiation. *Nat. Commun.* **10**, 2755 (2019).
10. S. Wu, S. Buckley, J. R. Schaibley, L. Feng, J. Yan, D. G. Mandrus, F. Hatami, W. Yao, J. Vučković, A. Majumdar, X. Xu, Monolayer semiconductor nanocavity lasers with ultralow thresholds. *Nature* **520**, 69–72 (2015).
11. S. Butun, S. Tongay, K. Aydin, Enhanced light emission from large-area monolayer MoS_2 using plasmonic nanodisc arrays. *Nano Lett.* **15**, 2700–2704 (2015).
12. P. Tonndorf, R. Schmidt, R. Schneider, J. Kern, M. Buscema, G. A. Steele, A. Castellanos-Gomez, H. S. J. van der Zant, S. M. de Vasconcellos, R. Bratschitsch, Single-photon emission from localized excitons in an atomically thin semiconductor. *Optica* **2**, 347–352 (2015).
13. C. Chakraborty, L. Kinnischtzke, K. M. Goodfellow, R. Beams, A. N. Vamivakas, Voltage-controlled quantum light from an atomically thin semiconductor. *Nat. Nanotechnol.* **10**, 507–511 (2015).
14. A. Srivastava, M. Sidler, A. V. Allain, D. S. Lembke, A. Kis, A. Imamoğlu, Optically active quantum dots in monolayer WSe_2. *Nat. Nanotechnol.* **10**, 491–496 (2015).
15. Y.-M. He, G. Clark, J. R. Schaibley, Y. He, M.-C. Chen, Y.-J. Wei, X. Ding, Q. Zhang, W. Yao, X. Xu, C.-Y. Lu, J.-W. Pan, Single quantum emitters in monolayer semiconductors. *Nat. Nanotechnol.* **10**, 497–502 (2015).
16. M. Koperski, K. Nogajewski, A. Arora, V. Cherkez, P. Mallet, J.-Y. Veuillen, J. Marcus, P. Kossacki, M. Potemski, Single photon emitters in exfoliated WSe_2 structures. *Nat. Nanotechnol.* **10**, 503–506 (2015).
17. S. Kumar, A. Kaczmarczyk, B. D. Gerardot, Strain-induced spatial and spectral isolation of quantum emitters in mono-and bilayer WSe_2. *Nano Lett.* **15**, 7567–7573 (2015).
18. C. Chakraborty, K. M. Goodfellow, A. N. Vamivakas, Localized emission from defects in $MoSe_2$ layers. *Opt. Mater. Express* **6**, 2081–2087 (2016).
19. B. Schuler, J.-H. Lee, C. Kastl, K. A. Cochrane, C. T. Chen, S. Refaely-Abramson, S. Yuan, E. van Veen, R. Roldán, N. J. Borys, R. J. Koch, S. Aloni, A. M. Schwartzberg, D. F. Ogletree, J. B. Neaton, A. Weber-Bargioni, How substitutional point defects in two-dimensional WS_2 induce charge localization, spin-orbit splitting, and strain. *ACS Nano* **13**, 10520–10534 (2019).
20. C. Kastl, C. T. Chen, R. J. Koch, B. Schuler, T. R. Kuykendall, A. Bostwick, C. Jozwiak, T. Seyller, E. Rotenberg, A. Weber-Bargioni, S. Aloni, A. M. Schwartzberg, Multimodal spectromicroscopy of monolayer WS_2 enabled by ultra-clean van der Waals epitaxy. *2D Mater.* **5**, 045010 (2018).
21. K. Kuhnke, C. Große, P. Merino, K. Kern, Atomic-scale imaging and spectroscopy of electroluminescence at molecular interfaces. *Chem. Rev.* **117**, 5174–5222 (2017).
22. R. Berndt, J. K. Gimzewski, P. Johansson, Inelastic tunneling excitation of tip-induced plasmon modes on noble-metal surfaces. *Phys. Rev. Lett.* **67**, 3796–3799 (1991).
23. S. W. Wu, G. V. Nazin, W. Ho, Intramolecular photon emission from a single molecule in a scanning tunneling microscope. *Phys. Rev. B* **77**, 205430 (2008).
24. P. Merino, C. Große, A. Rosławska, K. Kuhnke, K. Kern, Exciton dynamics of C_{60}-based single-photon emitters explored by hanbury brown–twiss scanning tunnelling microscopy. *Nat. Commun.* **6**, 8461 (2015).
25. B. Doppagne, M. C. Chong, H. Bulou, A. Boeglin, F. Scheurer, G. Schull, Electrofluorochromism at the single-molecule level. *Science* **361**, 251–255 (2018).
26. B. Doppagne, M. C. Chong, E. Lorchat, S. Berciaud, M. Romeo, H. Bulou, A. Boeglin, F. Scheurer, G. Schull, Vibronic spectroscopy with submolecular resolution from stm-induced electroluminescence. *Phys. Rev. Lett.* **118**, 127401 (2017).
27. T. Lutz, C. Große, C. Dette, A. Kabakchiev, F. Schramm, M. Ruben, R. Gutzler, K. Kuhnke, U. Schlickum, K. Kern, Molecular orbital gates for plasmon excitation. *Nano Lett.* **13**, 2846–2850 (2013).
28. A. Yu, S. Li, H. Wang, S. Chen, R. Wu, W. Ho, Visualization of nanoplasmonic coupling to molecular orbital in light emission induced by tunneling electrons. *Nano Lett.* **18**, 3076–3080 (2018).
29. A. Rosławska, P. Merino, C. Große, C. C. Leon, O. Gunnarsson, M. Etzkorn, K. Kuhnke, K. Kern, Single charge and exciton dynamics probed by molecular-scale-induced electroluminescence. *Nano Lett.* **18**, 4001–4007 (2018).
30. P. Merino, A. Rosławska, C. Große, C. C. Leon, K. Kuhnke, K. Kern, Bimodal exciton-plasmon light sources controlled by local charge carrier injection. *Sci. Adv.* **4**, eaap8349 (2018).
31. K. Kimura, K. Miwa, H. Imada, M. Imai-Imada, S. Kawahara, J. Takeya, M. Kawai, M. Galperin, Y. Kim, Selective triplet exciton formation in a single molecule. *Nature* **570**, 210–213 (2019).
32. D. Pommier, R. Bretel, L. E. Parra López, F. Fabre, A. Mayne, E. Boer-Duchemin, G. Dujardin, G. Schull, S. Berciaud, E. L. Moal, Scanning tunneling microscope-induced excitonic luminescence of a two-dimensional semiconductor. *Phys. Rev. Lett.* **123**, 027402 (2019).
33. N. Krane, C. Lotze, J. M. Läger, G. Reecht, K. J. Franke, Electronic structure and luminescence of quasi-freestanding MoS_2 nanopatches on Au(111). *Nano Lett.* **16**, 5163–5168 (2016).
34. R. Beams, P. Bharadwaj, L. Novotny, Electroluminescence from graphene excited by electron tunneling. *Nanotechnology* **25**, 055206 (2014).
35. S. Barja, S. Refaely-Abramson, B. Schuler, D. Y. Qiu, A. Pulkin, S. Wickenburg, H. Ryu, M. M. Ugeda, C. Kastl, C. Chen, C. Hwang, A. Schwartzberg, S. Aloni, S.-K. Mo, D. F. Ogletree, M. F. Crommie, O. V. Yazyev, S. G. Louie, J. B. Neaton, A. Weber-Bargioni, Identifying Substitutional Oxygen as a Prolific Point Defect in Monolayer Transition Metal Dichalcogenides with Experiment and Theory. *Nat. Commun.* **10**, 3382 (2019).
36. B. Schuler, D. Y. Qiu, S. Refaely-Abramson, C. Kastl, C. T. Chen, S. Barja, R. J. Koch, D. F. Ogletree, S. Aloni, A. M. Schwartzberg, J. B. Neaton, S. G. Louie, A. Weber-Bargioni, Large Spin-Orbit Splitting of Deep In-Gap Defect States of Engineered Sulfur Vacancies in Monolayer WS_2. *Phys. Rev. Lett.* **123**, 076801 (2019).
37. P. Johansson, R. Monreal, P. Apell, Theory for light emission from a scanning tunneling microscope. *Phys. Rev. Lett.* **42**, 9210–9213 (1990).
38. R. Alvarez-Puebla, L. M. Liz-Marzán, F. J. Garcia de Abajo, Light concentration at the nanometer scale. *J. Phys. Chem. Lett.* **1**, 2428–2434 (2010).
39. C. C. Leon, O. Gunnarsson, D. G. de Oteyza, A. Rosławska, P. Merino, A. Grewal, K. Kuhnke, K. Kern, Single photon emission from a plasmonic light source driven by a local field-induced coulomb blockade. *ACS Nano* **14**, 4216–4223 (2020).
40. F. J. Giessibl, High-speed force sensor for force microscopy and profilometry utilizing a quartz tuning fork. *Appl. Phys. Lett.* **73**, 3956 (1998).
41. F. Mohn, B. Schuler, L. Gross, G. Meyer, Different tips for high-resolution AFM and STM imaging of single molecules. *Appl. Phys. Lett.* **102**, 073109 (2013).
42. J. Bardeen, Tunnelling from a many-particle point of view. *Phys. Rev. Lett.* **6**, 57–59 (1961).
43. J. Tersoff, D. R. Hamann, Theory of the scanning tunneling microscope. *Phys. Rev. B* **31**, 805–813 (1985).
44. J. K. Gimzewski, B. Reihl, J. H. Coombs, R. R. Schlittler, Photon emission with the scanning tunneling microscope. *Z. Phyz. B* **72**, 497–501 (1988).
45. P. Johansson, Light emission from a scanning tunneling microscope: Fully retarded calculation. *Phys. Rev. B* **58**, 10823–10834 (1998).
46. J. Aizpurua, S. P. Apell, R. Berndtt, Role of tip shape in light emission from the scanning tunneling microscope. *Phys. Rev. B* **62**, 2065–2073 (2000).
47. G. Hoffmann, J. Aizpurua, P. Apell, R. Berndt, Inffluence of tip geometry in light emission from the scanning tunnelling microscope. *Surf. Sci.* **482-485**, 1159–1162 (2001).
48. N. Nilius, N. Ernst, H.-J. Freund, Tip influence on plasmon excitations in single gold particles in an stm. *Phys. Rev. B* **65**, 115421 (2002).
49. K. Meguro, K. Sakamoto, R. Arafune, M. Satoh, S. Ushioda, Origin of multiple peaks in the light emission spectra of a au(111) surface induced by the scanning tunneling microscope. *Phys. Rev. B* **65**, 165405 (2002).
50. J. Lambe, S. L. McCarthy, Light emission from inelastic electron tunneling. *Phys. Rev. Lett.* **37**, 923–925 (1976).
51. B. N. J. Persson, A. Baratoff, Theory of photon emission in electron tunneling to metallic particles. *Phys. Rev. Lett.* **68**, 3224–3227 (1992).
52. J. D. Jackson, *Classical Electrodynamics* (Wiley, 1999).
53. F. J. García de Abajo, Optical excitations in electron microscopy. *Rev. Mod. Phys.* **82**, 209–275 (2010).
54. L. A. Blanco, F. J. García de Abajo, Spontaneous light emission in complex nanostructures. *Phys. Rev. B* **69**, 205414 (2004).
55. R. Loudon, *The Quantum Theory of Light* (Oxford Univ. Press, 2000).
56. L. Novotny, B. Hecht, *Principles of Nano-Optics* (Cambridge Univ. Press, 2006).
57. E. J. C. Dias, F. J. García, de Abajo, Fundamental limits to the coupling between light and 2d polaritons. *ACS Nano* **13**, 5184–5197 (2019).
58. F. J. García de Abajo, Nonlocal effects in the plasmons of strongly interacting nanoparticles, dimers, and waveguides. *J. Phys. Chem. C* **112**, 17983–17987 (2008).
59. E. M. Purcell, Spontaneous emission probabilities at radio frequencies. *Phys. Rev.* **69**, 681 (1946).
60. F. J. García de Abajo, M. Kociak, Probing the photonic local density of states with electron energy loss spectroscopy. *Phys. Rev. Lett.* **100**, 106804 (2008).
61. M. Esmann, S. F. Becker, J. Witt, J. Zhan, A. Chimeh, A. Korte, J. Zhong, R. Vogelgesang, G. Wittstock, C. Lienau, Vectorial near-field coupling. *Nat. Mater.* **14**, 698–704 (2019).
62. K. V. Emtsev, A. Bostwick, K. Horn, J. Jobst, G. L. Kellogg, L. Ley, J. L. Mc Chesney, T. Ohta, S. A. Reshanov, J. Röhrl, E. Rotenberg, A. K. Schmid, D. Waldmann, H. B. Weber, T. Seyller, Towards wafer-size graphene layers by atmospheric pressure graphitization of silicon carbide. *Nat. Mater.* **8**, 203–207 (2009).

Acknowledgments

Funding: This work was supported as part of the Center for Novel Pathways to Quantum Coherence in Materials, an Energy Frontier Research Center funded by the U.S. Department of Energy, Office of Science, Basic Energy Sciences. This work was performed at the Molecular Foundry supported by the Office of Science, Office of Basic Energy Sciences, of the U.S. Department of Energy under contract no. DE-AC02-05CH11231. B.S. acknowledges support from the Swiss National Science Foundation under project number P2SKP2_171770. C.K.

Downloaded from http://advances.sciencemag.org/ on October 19, 2020

acknowledges support by the Bavaria California Technology Center (BaCaTeC) and the International Graduate School of Science and Engineering (IGSSE) via project "CommOnChip." A.W.-B. was supported by the U.S. Department of Energy Early Career Award. F.J.G.A. acknowledges support from the Spanish MINECO (MAT2017-88492-R and SEV2015-0522), the European Research Council (advanced grant 789104-eNANO), the Catalan CERCA Program, and the Fundació Privada Cellex. **Author contributions:** B.S. and A.W.-B. conceived the experiments. B.S. and K.A.C. conducted the SPM measurements. C.K. and A.M.S. synthesized the samples. B.S., E.S.B., E.W., and N.J.B. constructed the optical detection setup. F.J.G.A. derived the theoretical framework. All authors discussed the results and contributed to the manuscript. **Competing interests:** The authors declare that they have no competing interests. **Data and materials availability:** All data needed to evaluate the conclusions in the paper are present in the paper and/or the Supplementary Materials. Additional data related to this paper may be requested from the authors.

Submitted 5 March 2020
Accepted 31 July 2020
Published 16 September 2020
10.1126/sciadv.abb5988

Citation: B. Schuler, K. A. Cochrane, C. Kastl, E. S. Barnard, E. Wong, N. J. Borys, A. M. Schwartzberg, D. F. Ogletree, F. J. García de Abajo, A. Weber-Bargioni, Electrically driven photon emission from individual atomic defects in monolayer WS_2. *Sci. Adv.* **6**, eabb5988 (2020).

Downloaded from http://advances.sciencemag.org/ on October 19, 2020

Science Advances

Electrically driven photon emission from individual atomic defects in monolayer WS_2

Bruno Schuler, Katherine A. Cochrane, Christoph Kastl, Edward S. Barnard, Edward Wong, Nicholas J. Borys, Adam M. Schwartzberg, D. Frank Ogletree, F. Javier García de Abajo and Alexander Weber-Bargioni

Sci Adv **6** (38), eabb5988.
DOI: 10.1126/sciadv.abb5988

ARTICLE TOOLS http://advances.sciencemag.org/content/6/38/eabb5988

SUPPLEMENTARY MATERIALS http://advances.sciencemag.org/content/suppl/2020/09/14/6.38.eabb5988.DC1

REFERENCES This article cites 59 articles, 5 of which you can access for free
http://advances.sciencemag.org/content/6/38/eabb5988#BIBL

PERMISSIONS http://www.sciencemag.org/help/reprints-and-permissions

Use of this article is subject to the Terms of Service

Science Advances (ISSN 2375-2548) is published by the American Association for the Advancement of Science, 1200 New York Avenue NW, Washington, DC 20005. The title *Science Advances* is a registered trademark of AAAS.

Copyright © 2020 The Authors, some rights reserved; exclusive licensee American Association for the Advancement of Science. No claim to original U.S. Government Works. Distributed under a Creative Commons Attribution NonCommercial License 4.0 (CC BY-NC).

Downloaded from http://advances.sciencemag.org/ on October 19, 2020